

Experimental study of the non-linear phase of the vortex ring instability.

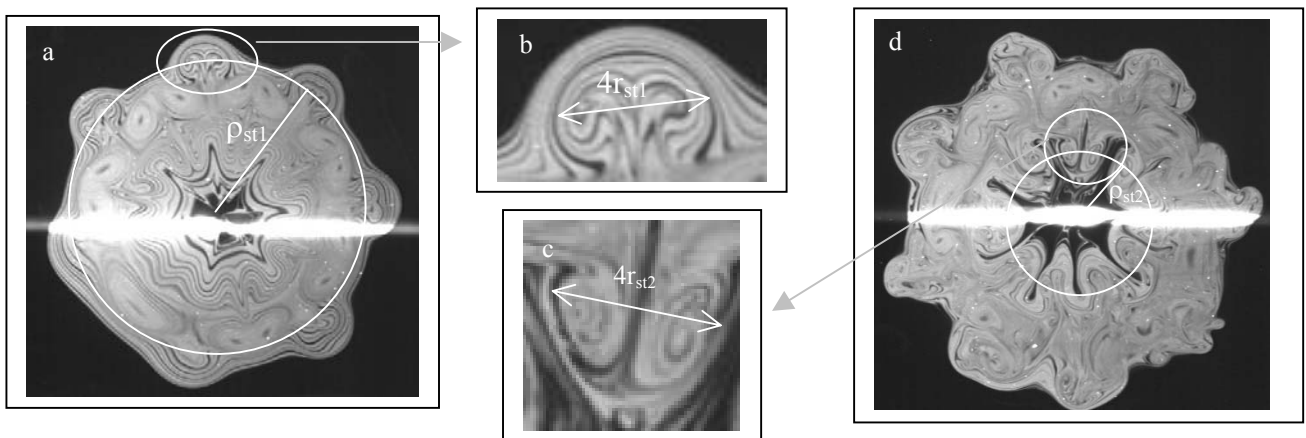
by

A. Dazin, P. Dupont and M. Stanislas

Laboratoire de Mécanique de Lille (UMR CNRS 8107),
Boulevard Paul Langevin, Cité Scientifique,
59655 Villeneuve d'ascq Cédex
E-Mail: Stanislas@ec-lille.fr.

ABSTRACT

The first stage of the instability of the vortex ring is linear and characterized by the growth of an azimuthal stationary wave which develops around the ring. Its origin, shape, number of waves and growth rate are predicted by theoretical works. Experimental and numerical results in viscous fluid fit well with those predictions based on an ideal fluid hypothesis. On the other hand, the next stages of the development of the instability (which are non-linear) are not well known. Only few phenomena are described, in an isolated way, in various partial contribution. The aim of this paper is to report a complete experimental investigation made on the non-linear phase of the instability of the vortex ring. The vortices were produced in water and their Reynolds number Re_p was varied from 2650 to 6100. Visualization were performed using Planar Laser Induced Fluorescence and measurements with 2D2C and 2D3C Particle Image Velocimetry. Based on a Fourier analysis of the results, it appears that the non-linear phase begins by the development of the harmonics of the linear mode (first unstable mode). But the growth of those harmonics is rapidly stopped by the development of low order modes. Then appear a $m = 0$ mode, which corresponds to a mean azimuthal velocity around the vortex. Simultaneously, secondary vortical structures develop all around the vortex in its peripheral zone (see figure below). Those vortical structures are linked with the ejection of vorticity in the wake of the vortex and they appear just before the transition toward turbulence. A tentative is made to place chronologically all these phenomena in order to propose a scenario from the end of the linear phase to turbulence.



Visualization of secondary structures 1 (a and b) and 2 (c and d).

Nomenclature

a : vortex core radius.

a_e : effective core radius; defined by $V = \frac{\Gamma}{4\pi R} \left(\ln \frac{8R}{a_e} - \frac{1}{4} \right)$.

a_i : inner core radius (distance from the core where the tangential velocity is maximal).

D_p : tube inner diameter.

h : distance between the laser sheet and the median plane of the vortex.

L_p : piston stroke.

n : number of unstable waves.

r = radial coordinate in the cylindrical coordinate system centred on the vortex ring.

R : vortex radius.

$Re_p = \frac{D_p U_p}{\nu}$: Reynolds number based on the piston velocity and the tube diameter.

$Re_0 = \frac{2RV}{\nu}$: Reynolds number based on the vortex velocity and diameter.

U_p : piston average velocity.

V : propagation speed of the ring.

$z_c = h/R$.

α : growth rate of the instability.

Γ : circulation of the ring.

θ : azimuthal coordinate in the cylindrical coordinate system centred on the vortex ring.

ν : viscosity

1- Introduction

The instability of the vortex ring starts with a linear phase whose origin and consequence have been well explored by theoretical (Widnall et al (1974), Widnall et Tsai (1977), Saffman (1978)), numerical (Shariff et al (1992)) and experimental works (Maxworthy (1972), Sullivan et al (1973), Maxworthy (1977), Didden (1977), Dazin (2003), Dazin (2004)). The linear phase is characterized by the development of an azimuthal stationary wave which develop around the vortex. Dazin (2003) shows that the growth of the linear wave ends abruptly. This points out the appearance of non-linear phenomena. Some of this non-linear phenomena have already been explored in previous studies. The most commonly observed phenomenon is the development of azimuthal velocities around the vortex ring. It was first observed by Maxworthy (1972). For high Reynolds number ($4.5 \cdot 10^4 < Re_p < 7.9 \cdot 10^4$), he observed dye azimuthal displacement near the vortex core. Away from the core, other azimuthal motions are observed but in the opposite direction. Naitoh et al (2002), for a vortex ring at $Re = 1600$, combining visualization and smoke wire technique, observed also azimuthal velocities. As for the Maxworthy study, the sign of the velocity is changed when going away from the core of the vortex. On the contrary to Maxworthy (1977) study, this phenomenon develops before the end of the azimuthal wave predicted by linear theory. Both authors distinguish two kinds of phenomena. The first one is a mean azimuthal velocity (corresponding to the zero order Fourier mode, called $m = 0$). The second one shows velocities of opposite direction in the inner and outer parts of the ring (mode $m = 1$). Shariff et al (1992), in a numerical study of the instability of vortex rings also observes the arising of a mean azimuthal velocity and of a mode $m = 1$. They also observe the growth of the harmonics of the linear mode. The non-linear phase is also characterized by the ejection of structures in the downstream part of the vortex, as observed by Schneider (1980) and Weigand and Gharib (1994). These authors suggest that those structures could be vortical ones and that this phenomena is the cause of the significant decrease of the vortex velocity and circulation during the non-linear phase. Vortical structures also appear (Didden (1977)) in the vortex core and in its peripheral part.

The other non-linear phenomenon are linked with generation of the vortex. Glezer (1988) observed a Kelvin-Helmoltz like instability in the wake of the vortex. Maxworthy (1977) has observe the creation of a second vortex (called piston vortex) when there is a brutal stop of the piston. This piston vortex (Allen and Auvity (2002)) can interact with the primary vortex and accelerate the unstable phenomena. As can be seen, the different studies concerning the non-linear phase of the instability report dissimilar phenomena. The aim of the work presented in this paper is, through an experimental investigation combining 2D2C and 2D3C Particle Image Velocimetry (PIV) and Planar Induced Fluorescence (PLIF), to find all this phenomena again, but also to regroup them in order to understand the different stages leading from the end of the linear phase to turbulence.

The experimental setup is presented in §2 and the results in §3. The conclusion (§4) gives the proposed chronology of those phenomena.

2- Experimental set-up

The present experiments were performed in water. The vortex rings were generated by pushing fluid throughout the cylindrical nozzle of a pipe, which is plunged into an aquarium (2.4m x 0.6m x 0.6m for the 2D2C PIV and visualisation experiments and 1m x 1m x 0,6m for the stereoscopic experiments). The inner diameter of the pipe is $D_p = 35$ mm. The pipe is connected to a pressurised tank. Between the pipe and the tank, an electromagnetic valve opens the circuit for an adjustable duration. A polystyrene piston is fitted into the pipe in order to isolate the flow in the aquarium from the perturbations of the generating system. The stroke of this piston is adjustable. By setting the tank pressure and the opening time of the valve, it is possible to control the velocity of the piston (figure 1a).

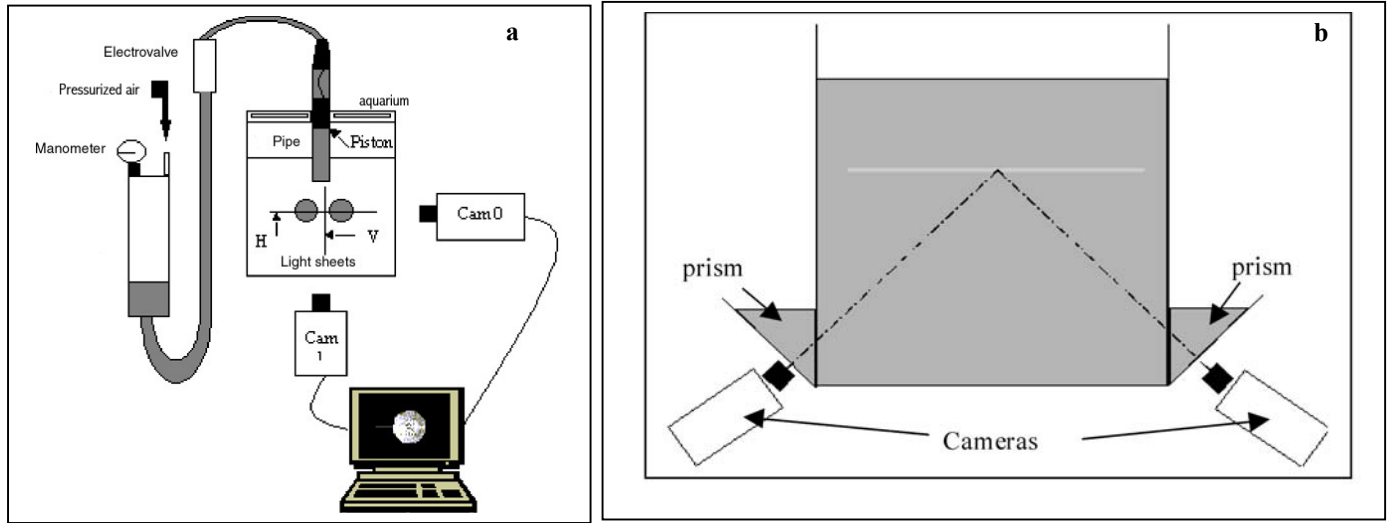


Figure 1 : Experimental set-up.

In the present set of experiment, the average piston velocity U_p was varied from 75 to 130 mm/s and the stroke to nozzle-diameter ratio L_p/D_p from 1.25 to 2.5. Consequently, the Reynolds number $Re_p = (U_p D_p)/\nu$ varied from 2625 to 5125. Table 1 gives the injection characteristics (the stroke to nozzle-diameter ratio and Reynolds number) of the vortices produced for the present experiments (vortices A to F for the visualisation, A' and C' for PIV experiments). This table also gives the circulation, propagation speed, radius, inner core radius and effective core radius of the vortex rings (the two last parameters need the knowledge of the velocity profile in the core and can be calculated only from the PIV results ; ie for the A' and C' vortices).

The inner core radius is defined as the distance from the centre of the core where the tangential velocity is maximum. The effective core radius is defined from the propagation speed by :

$$V = \frac{\Gamma}{4\pi R} \left(\ln \frac{8R}{a_e} - \frac{1}{4} \right)$$

(Saffman (1978)).

Table 1 : Vortices and injection characteristics.

	U_p (mm/s)	L_p/D_p	Re_p	Γ (mm.s ⁻²)	V (mm.s ⁻¹)	R (mm)	a_e (mm)	a_i (mm)
A	110	1.25	3800	6500	52	24	13.4	
B	145	1.25	5125	8400	66	24.25	13.8	
C	140	1.95	4900	6500	64	24.5	7.4	
D	75	2.4	2650	4800	65	24	8.9	
E	110	2.5	3800	6500	45	24.75	9.6	
F	145	2.5	5070	8900	58	24.75	10.5	
A'	100	1.25	3500	6000	57	24	8.5	8
C'	132	1.9	4600	6500	65	24.25	7.2	9

2D2C PIV and PLIF records were obtained in the symmetry plane of the vortex ring (V) and in a plane normal to its axis (H) (figure 1a) and the stereo PIV records only in the (H) plane. The video recordings were performed with two identical CCD cameras (Pulnix TM-9701, 768*484 pixels, 30 Hz framing rate). One was placed on one side of the aquarium and the other one was under the aquarium for the 2D2C PIV and PLIF experiments (figure 1a). These cameras were placed on both sides of the aquarium for stereo PIV experiments (figure 1b). Liquid prisms were attached to the lateral walls to reduce optical aberrations. The video signals were digitised by means of an ICPCI board in a PC computer. The visualisation results are sets of simultaneous images in the two planes showing the different steps of the instability at a rate of 30 Hz. For the analysis of the PIV records, the cross-correlation technique was used with a correlation window size of 32x32 pixels (2D2C PIV) or 16x16 pixels (stereo PIV) and an overlapping of 50%. Correlation peaks were fitted with a three points gaussian model. The results consist of fields of 48x26 (PIV 2D2C) or 80x40 (2D3C) velocity vectors with a temporal resolution of 15 fields per second. The field of view was 195x150 mm² in the symmetry plane (V) and 110x85 mm² in the plane normal to the axis (H) for the 2D2C PIV experiments and 200*100 mm² for the stereo PIV experiments. The measurement uncertainty was determined for a quiescent flow. It gives $\varepsilon_{rms} \approx 0.075$ pixel (about 1% of the vortex velocity) for 2D2C PIV and $\varepsilon_{rms} \approx 0.15$ pixel (about 2% of the vortex velocity) for stereo PIV experiments. By taking into account the classical parameters influencing the accuracy (particle size and density, loss of particles, velocity gradients), the uncertainty on the velocity measurement is about 5% for the present experiments

To conclude this section, the parameters used to locate the velocity maps are presented. The time origin is at the opening of the electrovalve. During one experiment in the (H) plane, the vortex is crossing the laser sheet. It is thus of interest to locate the measurement plane with respect to the ring : the distance h between the laser sheet and the median plane of the vortex (the plane that is containing the cores' centre) is introduced (figure 2).

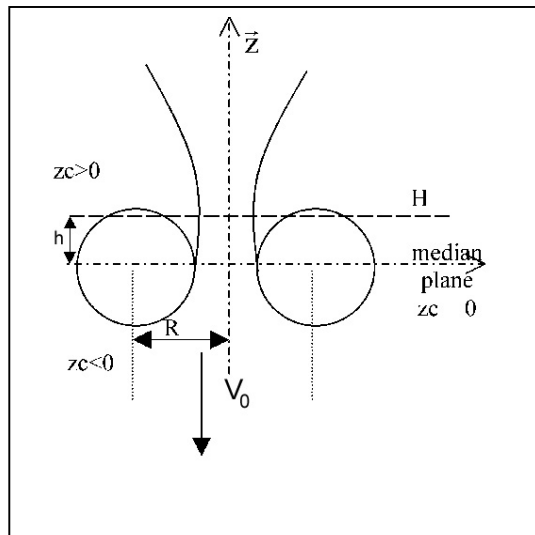


Figure 2 : Vortex characteristics.

In each figure are given the time t of the record and the non-dimensional position $zc = h/R$. zc is positive in the downstream part of the vortex and negative in the upstream part.

3- Results.

3-1. Scenario of the non-linear phase.

The linear phase of the instability is characterised by the growth of a three-dimensional stationary wave which develops around the ring. This wave develops on both axial, radial and azimuthal velocities but grows with a lag on azimuthal velocities. The first non-linear phenomena is the development of harmonics of the waves of the linear phase. But these harmonics stay at a low level and then decrease because of the development of low order modes. Simultaneously, a mean azimuthal velocity develops and secondary vortical structures arise in the peripheral zones of the vortex. The development of the structures involves the ejection of vorticity in the wake of the vortex and leads rapidly to turbulence. Those various phenomena are describe in the following parts. The linear phase of the instability has already been well describe (Dazin (2003)), but some informations about it are reminded (§ 3-2) before the description of the non-linear phenomena. Some of them (development of harmonics, of low order modes and of a mean azimuthal velocity) are mainly visible on Fourier spectra (§ 3-3). The other phenomena (secondary vortical structures and vortex shedding) are presented in § 3-4.

3-2 Linear phenomena.

The linear phase of the instability is characterised by the growth of an azimuthal non-progressive wave. It appears in the form alternative spots of low and high speed on the velocity maps in the H plane as illustrated for radial velocities in figure 3a. A Fourier transform of the velocities extracted on a circle centred on the vortex axis shows the band of linear unstable modes that develops (figure 3b), as predicted by the theory (Saffman (1978)).

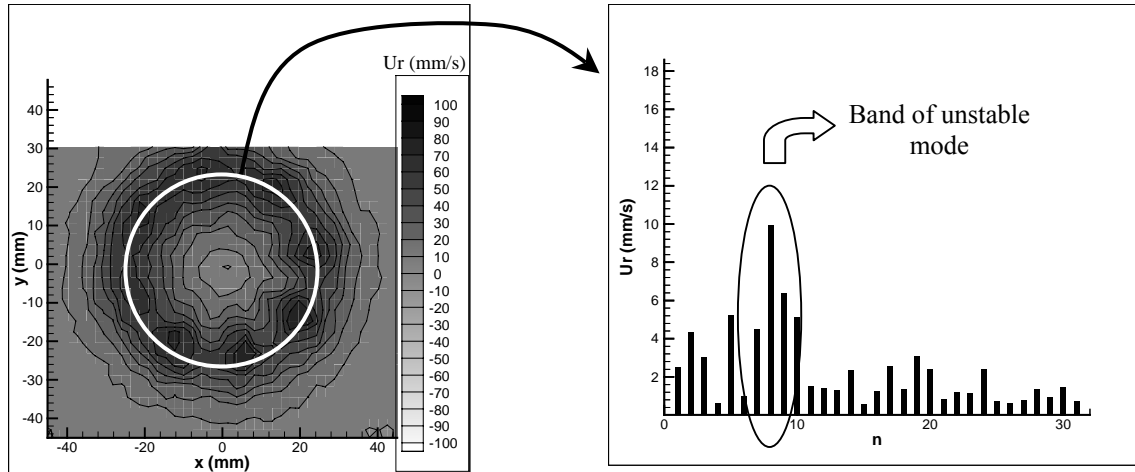


Figure 3: Radial velocity in the H plane (a) and the associated Fourier spectra.

The wave on azimuthal velocities has a phase difference of 90° with the wave on the radial ones. So, the velocity maps show consecutively zones of (figure 4):

- positive radial velocities,
- positive azimuthal velocities,
- negative radial velocities,
- negative azimuthal velocities.

Consequently, streamlines start from the vortex centre, and, when arriving at its periphery, turn back to the centre.

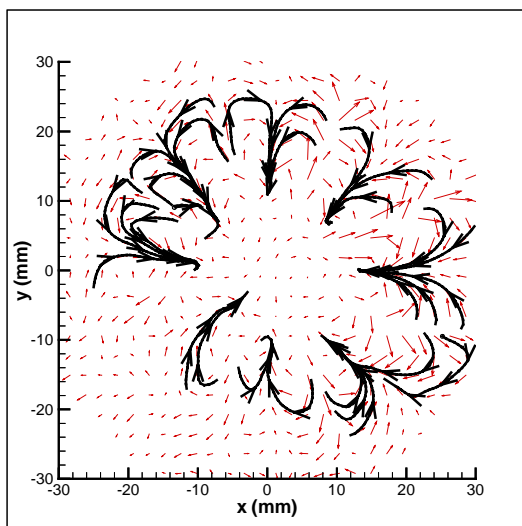


Figure 4: Velocity map in the H plane

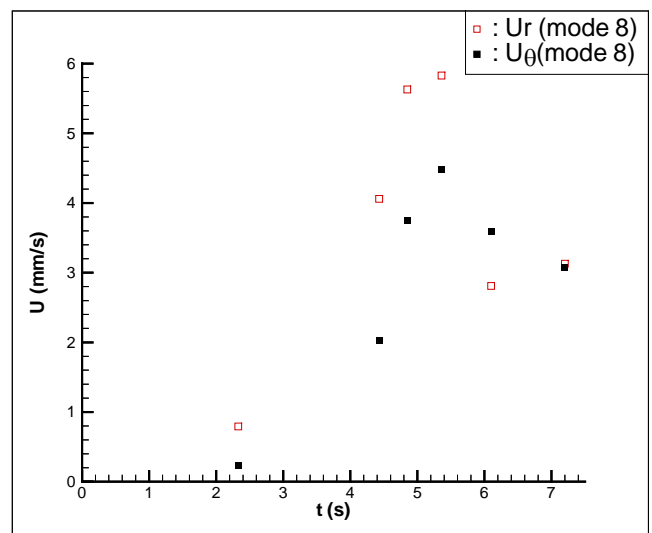


Figure 5: Comparison of the wave amplitude of radial and azimuthal velocity

The amplitude of the linear mode of radial and azimuthal velocities is plotted as a function of time on figure 5. They both present an exponential growth phase (until $t = 4.8$ s), predicted by the theory. Nevertheless, the wave on azimuthal velocities develops with a lag compared to the radial velocities. Both of them decrease strongly after $t = 4.8$ s, because of the arising of non-linear phenomena.

3-3. Modification of the Fourier Spectra.

3-3.1 Harmonics.

During the non-linear phase of the instability, harmonics of the linear modes develop. This can be seen on figure 6 for the A' vortex. The linear phase is characterized by the arising of a band of unstable modes around $n = 8$. During the non-linear phase, bands of modes develop also around $n = 16$ and in a minor degree around $n = 24$.

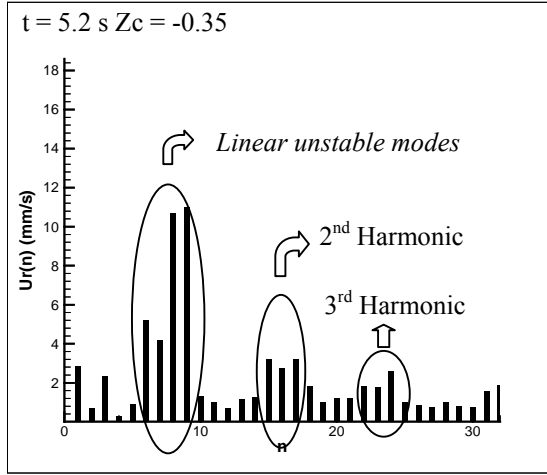


Figure 6: Harmonics of the unstable modes of the linear phase.

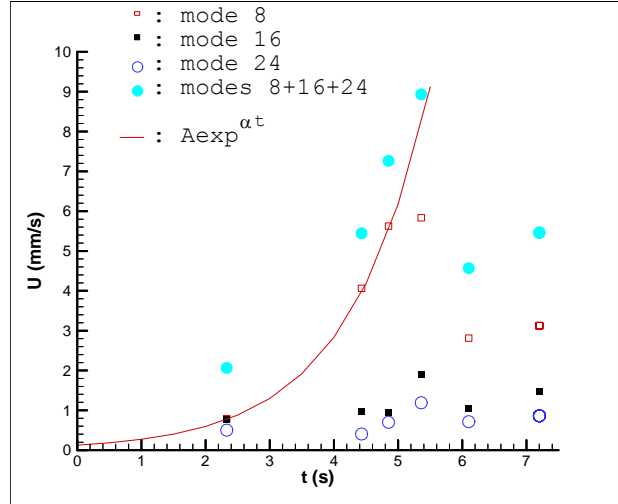


Figure 7: Evolution of the first unstable mode and of its harmonics.

To quantify these harmonics and compare them to the linear mode, their amplitude can be plotted as a function of time for the A' vortex (figure 7). The linear mode is $n = 8$. The beginning of its evolution is exponential. This corresponds to the development predicted by the linear theory. But the amplitude of this wave reaches a maximum at about $t = 4,8$ s. Simultaneously, the harmonics of this mode start a slight development and the harmonic summation has still an exponential growth. This is a classical phenomenon of instabilities: the most powerful mode transfers its energy towards its harmonics. But rapidly, the linear mode and its harmonics start a decrease. So, the energy transfer towards the harmonics ends quickly and is not the dominant phenomenon. In fact, the linear mode decrease is occurring at the same time as another phenomenon observed on Fourier spectrum: the arising of low order modes.

3-3.2 Low order modes

The development of low order modes is visible on the radial, axial and azimuthal velocity spectrum. It is illustrated for radial velocities in figure 8. To evidence their development, the evolution of five lower modes is compared to that of the linear mode in figure 9. The five modes have a similar evolution. They stay at a low level during the exponential growth of the linear mode. But just when this one reaches its maximum and starts to decrease, the low order modes develop strongly and then decrease slightly.

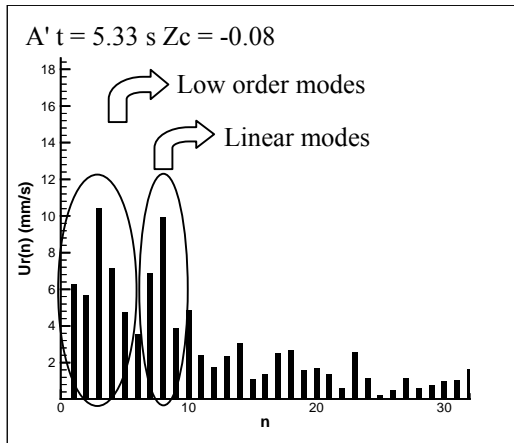


Figure 8: Low order modes on radial velocities

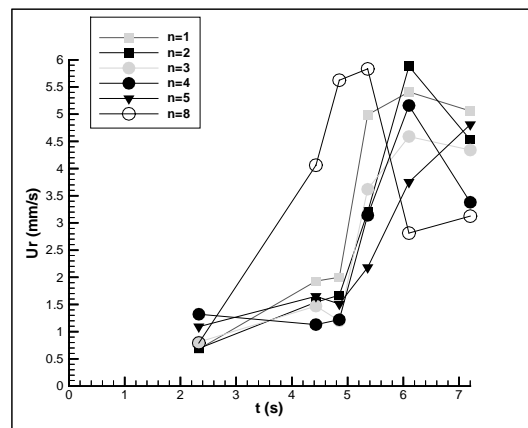


Figure 9: Evolution of the first linear mode and of the low order modes.

3-3.3 Mean azimuthal velocity.

Initially, there is no mean azimuthal velocity in the vortex. This is also true during the first stage (linear phase) of the instability. Such a velocity grows during the non-linear phase. Its appear in the form of a mode $m = 0$ on the Fourier spectra. This mean azimuthal velocity develops near the core centres as well as far from it, as shown in figure 10.

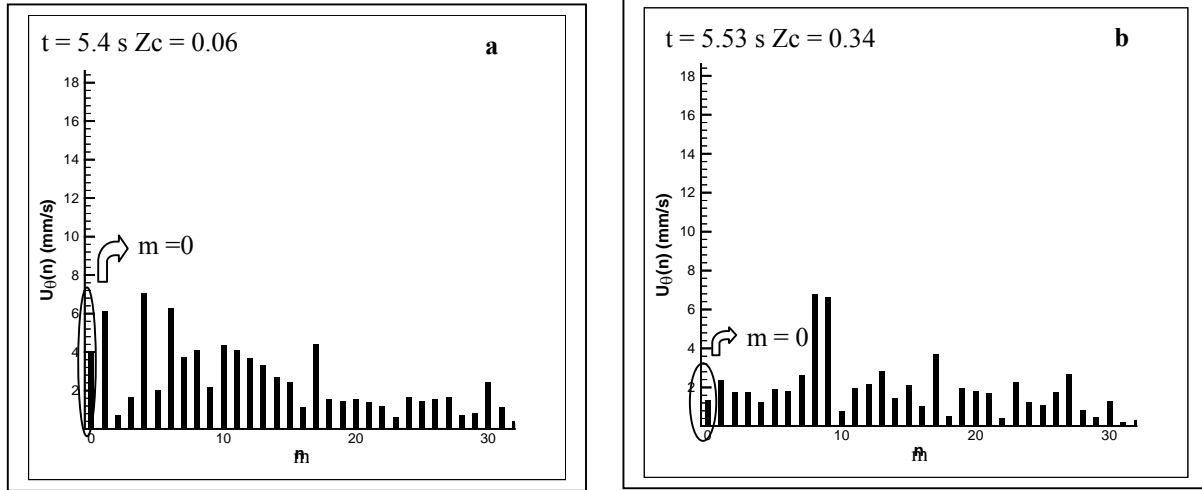


Figure 10: Development of the mean azimuthal velocity ($m=0$).

In figure 11, the Fourier mode amplitude is plotted as a function of Z_c .

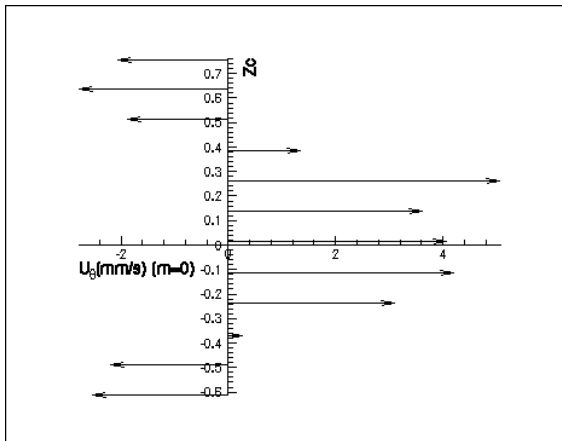


Figure 11: Amplitude of the mean azimuthal velocity as a function of Z_c .

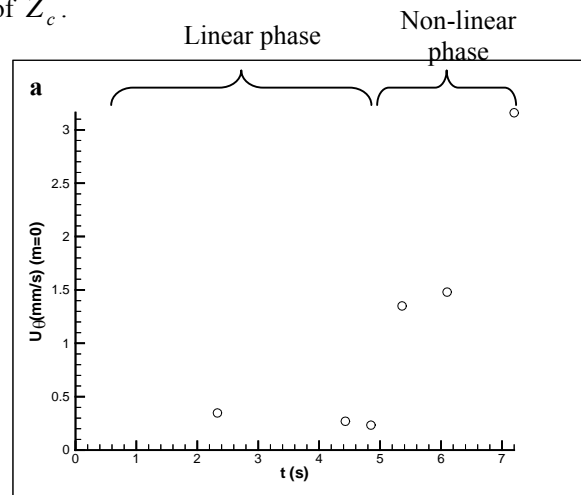


Figure 12: Development of the mean azimuthal velocity.

The mean azimuthal velocity is of opposite sign near the vortex core and far from it. The sign change takes place around $Z_c \approx 0.5$. This result is in agreement with the observation from Naitoh et al (2002). But, they estimate those velocities at 12 % of the vortex translation speed whereas our results give 7 %. The development of these azimuthal velocities is plotted figure 12. It shows that they are nearly zero during the linear phase of the instability. They then develop rapidly.

3-4. Secondary vortical structures and vortex shedding.

3-4-1 Secondary structures.

During the last phase of the instability, secondary vortical structures appear. The first ones (st1) develop in the outer part of the vortex. They are clearly visible on PLIF results in the (H) plane (figure 13 a,b). They are composed of two contra-rotative structures. They look like mushrooms developing all around the vortex. Later and nearer to the axis of the vortex appear other secondary structures called "secondary structures 2". These structures are also formed by pairs of two contra-rotative structures (figure 13 c, d). The distance ρ_{st} from the vortex core, the size r_{st} and the circulation Γ_{st}

of both types of structures have been estimated. These values are non-dimensionalised in ρ_{st}^* , r_{st}^* and Γ_{st}^* by the vortex ring radius R_0 and circulation Γ_0 (Table 2).

Table 2: Secondary structures 1 characteristics.

ρ_{st1}^*	r_{st1}^*	Γ_{st1}^*	ρ_{st2}^*	r_{st2}^*	Γ_{st2}^*
1.38	0.21	0.047	0.71	0.21	0.063

They appear to be 5 times smaller than the ring, and their circulation about 20 times lower.

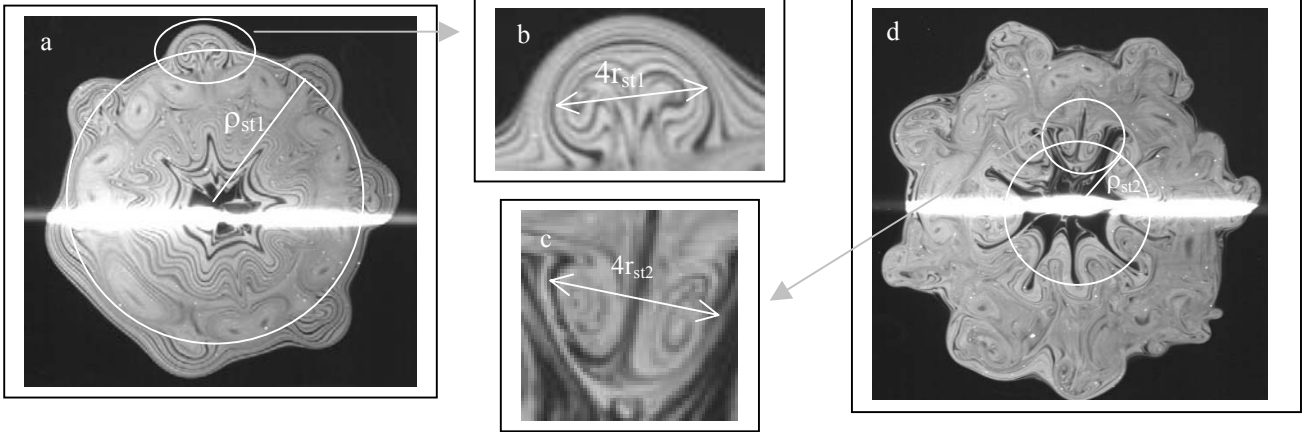


Figure 13: Visualization of secondary structures 1 (a and b) and 2 (c and d).

Their aspect seems to be similar to the structures observed in the last phase of the interaction of a vortex ring with a piston vortex and in the instability of a vortex ring generated by a water drop. This would show the similarity of the vortex ring instability mechanisms whatever the generation technique might be. Allen and al (2002) suggest that these structures originate from the upstream part of the vortex and then roll-up around the vortex. The present visualizations show a somewhat different mechanism. Figure 5 show that, although these vortex structures are not visible in the upstream part of the vortex, we can see them in the median plane.

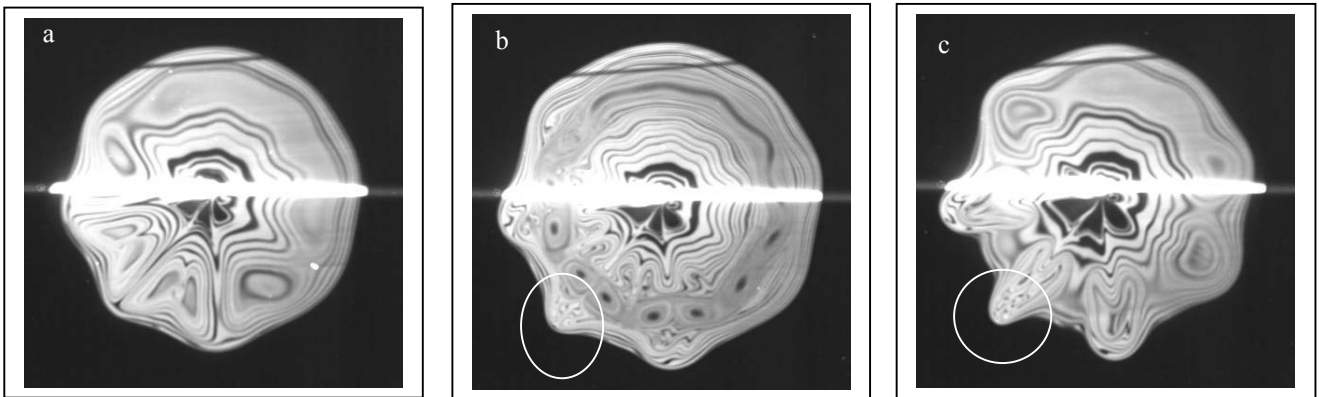


Figure 14: Vortex C - Z = 233 mm - a: t = 3.67 s, Zc = -0.31 - b: t = 3.8 s, Zc = 0 - c: 3.93 s Zc = 0.31

Actually, it seem that they originate from the median plane of the vortex and then wrap progressively around the whole vortex.

3-4.2 Ejection of vorticity.

When the (V) plane cuts these secondary structures, ejection of dye is evidenced in the downstream part of the vortex and axial vorticity in the H plane PIV results is observed in the wake.

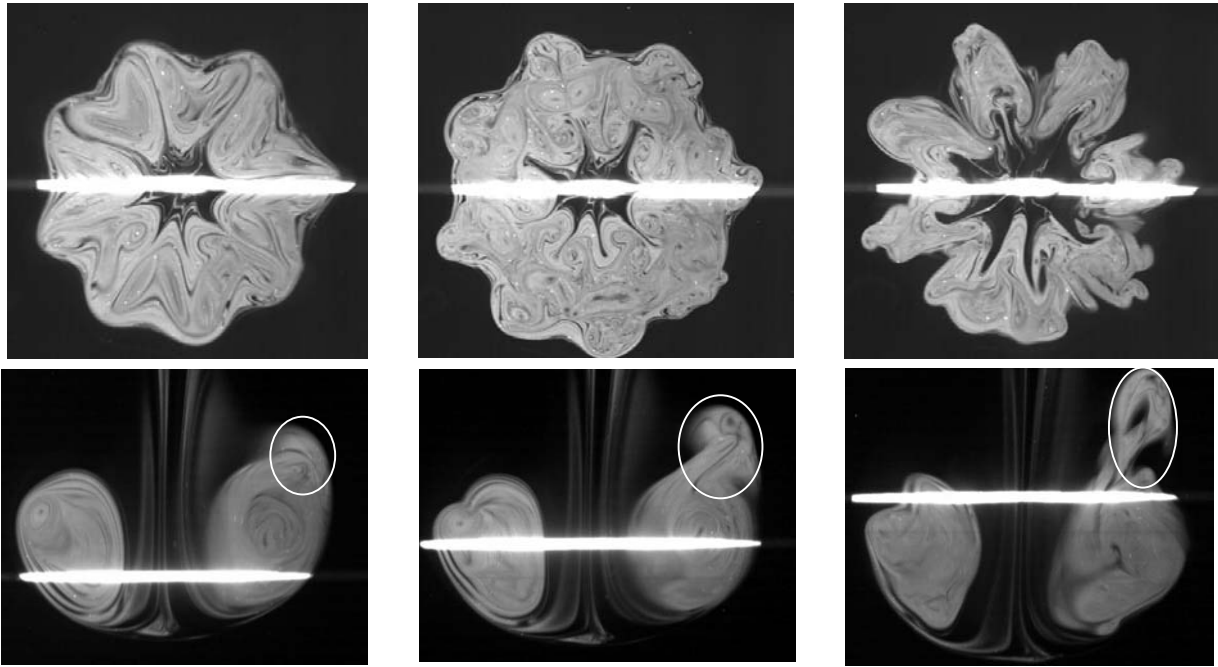


Figure 15 : dye ejections in the wake of the vortex.

This indicates that the secondary vortices are linked to vorticity ejections with a strong axial component. Those ejections must be one the major cause of the circulation decrease observed during the non-linear phase of the instability.

4- Conclusion

A complete experimental investigation has been managed to study the non-linear phase of the instability of vortex ring. This study has been made by Planar Laser Induced Fluorescence in two planes, 2D2C Particle Image Velocimetry in two planes and 2D3C Particle Image Velocimetry in one plane. This evidences various phenomena occurring after the exponential growth of the wave, predicted by linear theories. They are placed chronologically on figure 16.

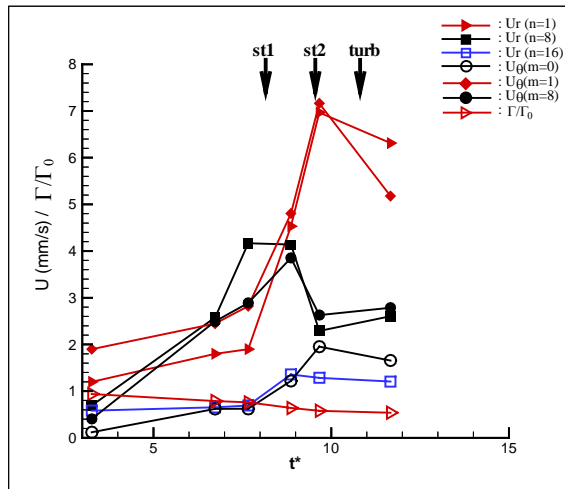


Figure 16: Linear phase chronology

The reference is the mode $n = 8$ for radial velocities, because it corresponds to the wave of the linear phase. The instability begins with the exponential growth of this wave. The mode $m = 8$, on azimuthal velocities has a development similar to the $n = 8$ mode on radial ones, but with a lag. When the exponential growth stops, harmonics of this wave develops. The harmonics are represented by the mode $n = 16$ in figure 16. They stay at a low level because their development is stopped by the arising of another phenomena, that is the development of low order modes (represented by the mode $m = 1$ for radial velocities and the mode $m = 1$ for azimuthal one). With the beginning of the non-linear phase, a mean azimuthal velocity (mode $m = 0$) arises also. Simultaneously, appear secondary structures 1 and 2 (st1 and st2 in figure 16). The development of these structures involves the ejection of vorticity in the wake of the vortex. This leads to the decrease of the circulation Γ of the vortex. Finally, the appearance of secondary structure 2 comes just before the transition towards turbulence. A picture of a turbulent vortex ring is given in figure 17.

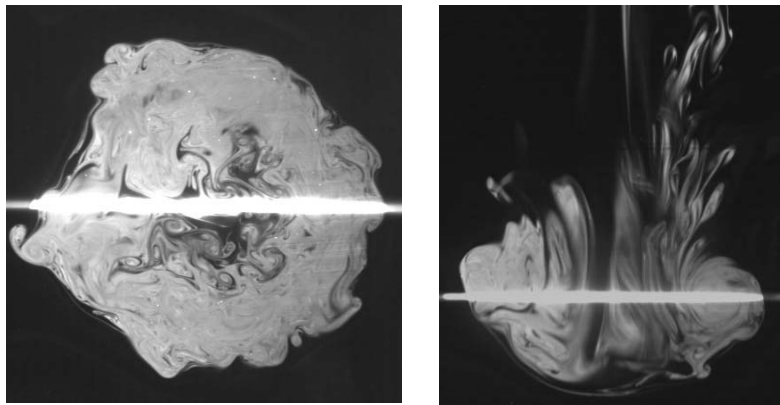


Figure 17 : Turbulent vortex ring.

References

- Allen J.J., Auvity B (2002) Interaction of a vortex ring with a piston vortex, JFM. 465 : 353-378.
- S.C. Crow (1970) Stability theory for a pair of trailing vortices. AIAA J 8: 2172.
- A. Dazin (2003) Caractérisation de l'instabilité du tourbillon torique par des méthodes optiques quantitatives. PhD Thesis, Université des Sciences et Technologies de Lille.
- A. Dazin, P. Dupont, M. Stanislas (2004) Experimental observation of the straining field responsible for vortex ring instability. CR – Mécanique 332 (231-236).
- N. Didden (1977) Untersuchung laminarer, instabiler Ringwirbel mittels Laser-Doppler-Anemometer. Mitt MPI und AVA, Göttingen, Nr. 64.
- Glezer A. (1988) The formation of vortex rings. Phys. Fluids A 31: 3532-42
- T. Maxworthy (1972) The structure and stability of vortex rings. J Fluid Mech 51: 15-32.
- T. Maxworthy (1977) Some experimental studies of vortex rings. J Fluid Mech 81: 465-495.
- T.Naitoh, N.Fukuda, T. Gotoh, H.Yamada, K.Nakajima. (2002) Experimental study of axial flow in a vortex ring. Physic of Fluids 14,1:143-148.
- K. Shariff, R. Verzicco, P. Orlandi (1992) A numerical study of three-dimensional vortex ring instabilities: viscous correction and early non-linear stage. J Fluid Mech 279: 351-375.
- P.G. Saffman (1978) The number of waves on unstable vortex rings. J Fluid Mech 84: 721-733.
- Schneider P.E.M. (1980) Sekundärerwirbelbildung bei Ringwirbeln und in Freistrahlen Z. Flugwiss.Weltraumforsch., 4,307-318.

J.P Sullivan, S.E Widnall, S. Ezekiel (1973) Study of vortex rings using a Laser Doppler Velocimeter. AIAA J 11: 1384-1389.

C.Y Tsai; S.E Widnall (1976) The stability of short waves on a straight vortex filament in a weak externally imposed strain field. J Fluid Mech 73: 721-733.

A. Weigand, M. Gharib., (1994) On the decay of a turbulent vortex ring. Phys.Fluids, 6,12 : 3806-3808.

S.E Widnall, J.P Sullivan, S. Ezekiel (1973) On the stability of vortex rings. Proc Roy Soc A. 332: 335-353.

S.E Widnall, D.B. Bliss, C.Y Tsai (1974) The instability of short waves on a vortex ring. J Fluid Mech 66: 35-47.

S.E Widnall, C.Y Tsai (1977) The instability of the thin vortex ring of constant vorticity. PH Trans Roy Soc London, a 287: 273-305.